Article details

Kadic M., Milton G.W., Hecke M.L. van & Wegener M. (2019), 3D metamaterials, Nature Reviews Physics 1: 198-210.
Doi: 10.1038/s42254-018-0018-y

3D metamaterials

*Muamer Kadic[1,2], Graeme W. Milton[3], Martin van Hecke[4,5] and Martin Wegener[2]**

Abstract | Metamaterials are rationally designed composites aiming at effective material parameters that go beyond those of the ingredient materials. For example, negative metamaterial properties, such as the refractive index, thermal expansion coefficient or Hall coefficient, can be engineered from constituents with positive parameters. Likewise, large metamaterial parameter values can arise from all-zero constituents, such as magnetic from non-magnetic, chiral from achiral and anisotropic from isotropic. The field of metamaterials emerged from linear electromagnetism two decades ago and today addresses nearly all conceivable aspects of solids, ranging from electromagnetic and optical, and mechanical and acoustic to transport properties — linear and nonlinear, reciprocal and non-reciprocal, monostable and multistable (programmable), active and passive, and static and dynamic. In this Review, we focus on the general case of 3D periodic metamaterials, with electromagnetic or optical, acoustic or mechanical, transport or stimuli-responsive properties. We outline the fundamental bounds of these composites and summarize the state of the art in theoretical design and experimental realization.

Inverse design
A design approach that defines the desired properties and searches for a microstructure exhibiting them; the inverse of taking a microstructure and calculating its properties.

[1]*Institut FEMTO-ST, CNRS, Université de Bourgogne Franche-Comté, Besançon, France.*

[2]*Institute of Nanotechnology and Institute of Applied Physics, Karlsruhe Institute of Technology (KIT), Karlsruhe, Germany.*

[3]*Department of Mathematics, University of Utah, Salt Lake City, UT, USA.*

[4]*AMOLF, Amsterdam, Netherlands.*

[5]*Huygens-Kamerlingh Onnes Lab, Universiteit Leiden, Leiden, Netherlands.*

**e-mail: martin.wegener@kit.edu*

https://doi.org/10.1038/s42254-018-0018-y

Although the idea of artificial composite materials has been around for more than a century, the notion of 3D metamaterials originated only approximately 20 years ago[1]. Since then, several factors have led to an explosion of interest. These include the unprecedented experimental ability to tailor complex 3D architectures, the growing awareness of the exceptional effective properties of 3D metamaterials and the tremendous progress in computer-aided design, including both numerical forward solutions and inverse design, for instance, via topology optimization[2]. Many theorists and experimentalists have turned from observers of nature into creative designers and engineers of artificial materials. In many cases studied so far, the properties of 3D metamaterials go beyond those of their ingredients, both qualitatively and quantitatively. Examples include negative refractive indices, diamagnetism and paramagnetism at optical frequencies, gigantic optical activity, exceptionally large nonlinear optical susceptibilities, non-reciprocal behaviour, negative mass densities, non-trivial mass density tensors, negative bulk moduli, negative acoustic indices, negative effective static volume compressibility, auxetic behaviour, pentamode behaviour, chiral and achiral micropolar behaviour, multistable and programmable mechanical parameters, sign reversal of the thermal expansion coefficient, sign reversal of the Hall coefficient and negative absolute mobilities. More examples are likely to emerge in the future.

The word metamaterial was used for the first time in a publication by Walser in 2001 (REF.[1]), but there is not yet a definition of metamaterials (FIG. 1) that is consistently used by all[3]. Most researchers would agree on the following loose definition: metamaterials are rationally designed composites made of tailored building blocks that are composed of one or more constituent bulk materials. The metamaterial properties go beyond those of the ingredient materials, qualitatively or quantitatively. (The prefix meta is derived from the ancient Greek word for beyond.) Rational design is a crucial aspect. It makes metamaterials distinct from other composites such as random foams, (naturally) patterned materials or mixtures. Rational design of the structure enables metamaterial properties to not only go beyond those of their ingredients but even be unprecedented, not found in nature or previously believed to be impossible. Of course, truly fundamental bounds, which may be different for 1D, 2D and 3D metamaterials, cannot be overcome. Using the notion of bulk material ingredients hides much of the atomic complexity and implies that the metamaterial building blocks or unit cells contain millions of atoms or more (FIG. 1)[4]. This aspect makes metamaterials distinct from ordinary crystals.

The above definition of metamaterials includes both periodic and non-periodic composites[5,6] (FIG. 1e). We focus on the periodic case, because the vast majority of metamaterials realized so far are actually periodic (FIG. 1f), and lattice translational invariance eases the discussion. Hence, the simplest example of a metamaterial is a single bulk material into which a rationally designed periodic porosity is introduced to achieve new properties.

Key points

- Metamaterials are rationally designed composites made of tailored building blocks, which are composed of one or more constituent bulk materials, leading to effective medium properties beyond those of their ingredients.
- Metamaterials thereby fulfil a long-standing dream of condensed matter physics to design materials on the computer to avoid tedious trial-and-error procedures and excessive experimentation.
- Although many 1D and 2D model architectures have been considered because of their ease of fabrication and reduced design complexity, the full potential of the metamaterial concept is opened up for 3D microstructures and nanostructures.
- In electromagnetism and optics, examples are effective diamagnetism and paramagnetism up to optical frequencies, impedance matching and duality, negative refractive indices, maximum electromagnetic chirality, perfect optical absorption and non-reciprocal propagation of electromagnetic waves without static magnetic fields.
- In acoustics and mechanics, examples are the complete flexibility in tailoring elastic parameters, chiral mechanical behaviour, sign reversal of the static effective compressibility, negative dynamic mass density, non-reciprocal sound propagation, broadband perfect sound absorption at the fundamental limit imposed by causality and highly nonlinear, multistable and programmable properties from linear elastic constituents.
- In transport, examples are highly anisotropic thermal conductance, sign reversal of the absolute mobility and the Hall coefficient, highly anisotropic Hall tensors, giant magnetoresistances and thermoelectric power factors that are enhanced by orders of magnitude.
- Future 3D material printers may achieve thousands of different effective metamaterial properties from only a small number of input material cartridges — in analogy to today's 2D graphical printers that mix thousands of colours from just three colour cartridges.

Several other notions used in the literature are more or less synonymous with the notion of metamaterials, notably architected materials (mainly used in the context of mechanics), designer matter, artificial materials or properties on demand. Metamaterials can be periodic in 1D, in 2D (metasurfaces[7]) or in 3D. This Review focuses on 3D metamaterials, as the possibilities of 1D and 2D structures are only a subset of the possibilities of 3D structures.

This Review is not organized chronologically but rather aims at emphasizing analogies and dissimilarities between electromagnetic and optical, mechanical and acoustic, and transport metamaterials. We leave out designed inhomogeneous metamaterial distributions, which, for example, enable invisibility cloaks and counterparts thereof, as this extension would deserve a review article of its own[8].

Effective parameters

In general, material properties are commonly described by effective macroscopic parameters that refer to fictitious continua (FIG. 1c)[5,9]. Examples include electrical conductivity, the Hall coefficient, electric permittivity or Young's modulus. In this manner, the complexity of a large system composed of many different components can be reduced. With the addendum that 'the properties of the metamaterial can be mapped onto effective-medium parameters', we sharpen our definition of metamaterials.

A sound mathematical basis for mapping periodic structures onto effective media or continua is the aim of homogenization theory[10–13]. Notably, it is currently not possible to homogenize an arbitrary periodic structure and map it onto an effective medium description, although high-frequency homogenization has been around for some years[9,10,14] and continues making progress in this direction[15]. Issues persist in regard to dealing with interfaces in an unambiguous way[13]. Homogenization becomes especially challenging in the limit that the material contrast of the ingredient materials is large or even diverges as the cell size shrinks to zero[16–18].

For many of the architectures discussed in this Review, mapping onto effective parameters is possible because a characteristic length scale, such as the wavelength or a transport length, is sufficiently large compared with the period or lattice constant. Effective continuum descriptions are not perfect[19–21], even for ordinary crystals. Furthermore, the mapping onto effective parameters is generally not unique. As a simple example, the optical properties of silicon can be described either by a frequency-dependent conductivity or by a frequency-dependent complex refractive index. For other architectures, it is not yet clear whether homogenization is possible. However, researchers have improved and conceptually expanded homogenization theories over the years and are continuing to do so. Hence, a structure that cannot be mapped onto an effective medium today may be able to tomorrow. Nevertheless, for other periodic architectures, homogenization does not make sense. For example, it is generally problematic to map the complex band structure of a photonic[22] or phononic[23] crystal, which may even contain topological bandgaps[24–26], onto effective material parameters — with the notable exception of the lowest bands in the long-wavelength limit.

Electromagnetic and optical metamaterials

Sometimes, bounds believed to be fundamental are actually not. The history of optical metamaterials provides an example of this. In their famous textbook[27], Landau and Lifshitz argue, on the basis of an inequality containing the atomic lattice constant $a < 1$ nm, that the relative magnetic permeability μ_r at optical frequencies is close to unity. In other words, the magnitude of the magnetic dipole density excited by the magnetic field of light is negligible. As a result, most optics textbooks essentially deal with only the relative electric permittivity ε_r, which describes an electric dipole density excited by the electric field of light.

This result is surprising. Faraday's law dictates that it is straightforward to induce a current by a time-varying magnetic field into a small coil of conducting wire with inductance L. The induced circulating current leads to a local magnetic dipole moment described by Ampère's circuit law. This moment can be made large by building a resonant LC circuit out of the coil and a capacitance C. Densely packing many such circuits into a 3D metamaterial leads to a large positive magnetic permeability μ_r^* below the resonance frequency and to $\mu_r^* < 0$ slightly above the resonance. Here, the symbol * denotes an effective property of the metamaterial. Many metamaterial unit cells (FIG. 2) include variations of this motif of a coil with one or more slits, that is, a split-ring resonator[28,29] (see FIG. 2a), also discussed in the literature under the names slotted-tube resonator[30], loop-gap resonator[31] or cut-wire pairs[32].

Topology optimization
A mathematical method that finds a microstructure that optimizes a set of parameters within a given design space and for given constraints.

Auxetic
An auxetic material shrinks laterally when being contracted axially. This behaviour corresponds to a negative Poisson ratio ν.

Pentamode
A pentamode material is a linear elastic 3D material for which five of the six possible modes of deformation cost no energy. Such materials behave approximately as a liquid.

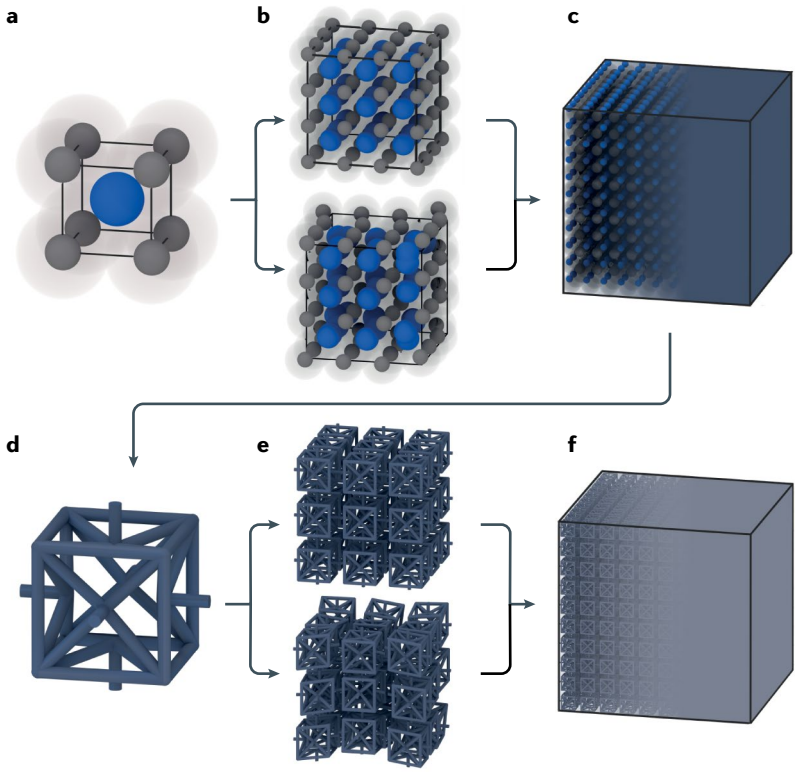

Fig. 1 | **From atoms via 3D materials to designed unit cells and 3D metamaterials.** **a**,**b** | Ordinary crystalline or amorphous materials are built up from atoms, which, in the case of crystals, form unit cells, as shown in panel **a**. **c** | To reduce the underlying complexity, materials are often treated as fictitious continuous media with associated effective parameters such as the electrical conductivity, the optical refractive index or the mechanical Young's modulus. **d** | These effective media are used as the ingredients for rationally designed artificial unit cells. **e** | Out of these, periodic or non-periodic 3D metamaterials are assembled. **f** | Again, to reduce complexity, metamaterials are mapped onto fictitious continuous media. Notably, the resulting effective metamaterial properties can go beyond those of the ingredient materials, qualitatively and/or quantitatively. This includes, for instance, the possibility of sign reversals and unbounded behaviour. The example unit cell shown in panel **d** leads to auxetic behaviour. Further examples are depicted in FIG. 2.

These resonators do not operate at arbitrarily large frequency, and it is not immediately intuitive why this is. Indeed, because the Maxwell equations are scalable, reducing the resonator size by a factor of ten also reduces the resonance wavelength by the same factor, which increases the resonance frequency by a factor of ten. The explanation for why this approach does not lead to operation at arbitrarily large frequency lies in the finite electron density and hence the finite plasma frequency of the constituent metal. This frequency is usually in the ultraviolet spectral region, making visible operation frequencies the operational limit. For driving frequencies approaching the plasma frequency, the metal properties deviate from those of an ideal conductor. The same physics can alternatively be expressed by the kinetic inductance[33], which adds to the Faraday inductance[34] and results in an upper limit of the LC circuit resonance frequency. In a circuit picture, further miniaturization towards the atomic scale is counterproductive, because the resistance R scales inversely with size; hence, as size decreases, damping increases, and the resonance gets washed out. In this situation, what is needed are metamaterials with lattice constants a much larger than the atomic scale (compared with FIG. 1) yet smaller than the operational wavelength λ, so that the structure can approximately be described as an effective medium with $\lambda / a \gg 1$. Landau and Lifshitz[27] did not foresee such systems (FIG. 2).

Negative refraction. The direction of the propagation of light can be changed by refraction at an interface between two materials. The refractive index n in Snell's law determines this change. Unusual behaviour can arise from negative n, from anisotropies and from chirality.

A positive n value means that the vectors of phase velocity $\boldsymbol{v}_p$ and energy velocity $\boldsymbol{v}_e$ or Poynting vector $\boldsymbol{S}$ (which are generally not parallel to the group velocity vector[35]) are parallel (more generally, $\boldsymbol{v}_p \cdot \boldsymbol{S} > 0$). If the refractive index is negative, they point in opposite directions[36–41] (more generally, $\boldsymbol{v}_p \cdot \boldsymbol{S} < 0$). This situation, which can occur if the real parts of ε_r and μ_r are both negative[36,37], is highly unusual (FIG. 2b). It created much of the early excitement in the field of metamaterials, in large part owing to the idea of perfect lenses[37] that overcome the Abbe diffraction limit.

However, losses occurring during propagation pose a problem for such metamaterials. Causality imposes that n has a finite imaginary part that represents propagation losses. Mathematically, the Kramers–Kronig relations[42] derived from causality make it possible to set the imaginary part of n to zero at a single finite frequency of light by introducing gain media[43–46]. However, unavoidable losses dramatically increase with increased detuning from this singular point. In passive structures based on metallic constituents, the inferred ratio of the negative real part to the imaginary part, the so-called figure of merit, has not exceeded values on the order of ten at optical frequencies[47]. This means that the light intensity decreases by more than 70% over just one wavelength of light, that is, a bulk metamaterial with an extent of many wavelengths is essentially opaque. In addition, the few experimental studies conducted were performed on 3D uniaxial structures, leading to anisotropic refractive index tensors, of which only some components were negative. Related restrictions apply to zero-index and epsilon-near-zero metamaterials[48–50].

An alternative route to negative refraction is given by anisotropic materials[51]. Hyperbolic (also known as indefinite) metamaterials[52–56] (FIG. 2c) are a special class of anisotropic media for which the electric permittivity is positive (dielectric) along one direction and negative (plasmonic) for the orthogonal direction. This leads to the isofrequency contours in momentum space, that is, the contours in momentum space along which frequency is constant, being hyperbolic. The hyperbola (in contrast to the ordinary circle or ellipse) makes it possible for light at a given frequency to access large momenta and hence to acquire unusually small effective wavelengths and super-resolution at optical frequencies.

Optical magnetism. Magnetism at elevated frequencies creates additional opportunities: $\mu_r^* \neq 1$ makes it possible to adjust the electromagnetic wave impedance $Z = \sqrt{\mu_0 \mu_r^* / (\varepsilon_0 \varepsilon_r^*)}$ independently of n, where μ_0 is the

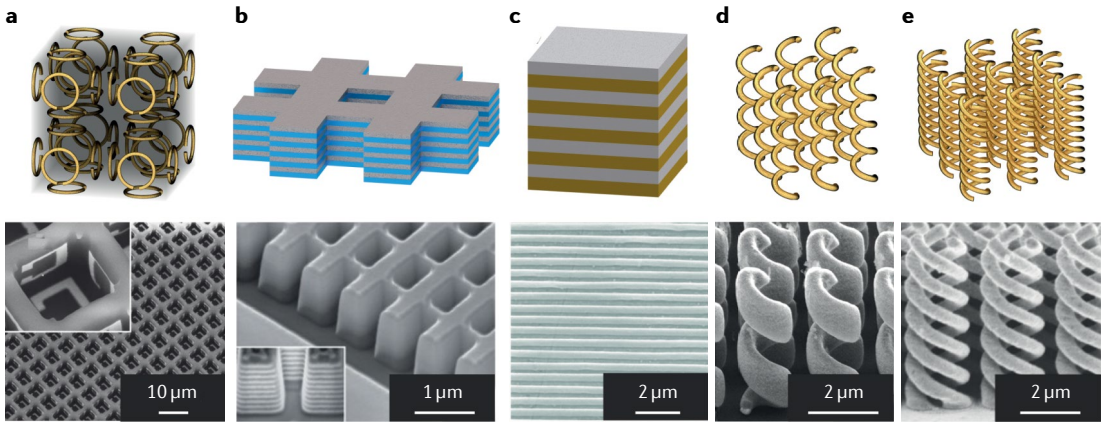

Fig. 2 | **Gallery of designed 3D optical metamaterial unit cells and corresponding experimental realizations.** **a** | An arrangement of metallic split-ring resonators leading to artificial magnetism. **b** | A fishnet arrangement for uniaxial negative refractive indices. **c** | An ABAB…AB laminate, which is a unit cell used in many metamaterials, including hyperbolic metamaterials. **d** | Helices providing chiral behaviour. **e** | Multiple intertwined helices for recovering three-fold rotational symmetry. Panel **a** is adapted with permission from REF.[192], Wiley-VCH. Panel **b** is adapted from REF.[47], Springer Nature Limited. Panel **c** is adapted from REF.[193], Springer Nature Limited. Panel **d** is adapted with permission from REF.[67], AAAS. Panel **e** is adapted with permission from REF.[70], OSA.

vacuum permeability and ε_0 is the vacuum permittivity. The impedance can be made equal to the vacuum impedance of $Z_0 = \sqrt{\mu_0 / \varepsilon_0} \approx 376.7\ \Omega$. By impedance matching, reflections from interfaces between a material and vacuum or air can be eliminated completely, regardless of the material's refractive index. In this situation, losses, which are a nuisance for negative refraction, can be turned into an advantage in perfect absorbers, which are materials that neither reflect nor transmit any light[57–60]. The idea of achieving impedance matching using balanced electric and magnetic responses is also key for the field of 2D Huygens metasurfaces[61]. For the case of $\mu_r^* < 0$ and $\varepsilon_r^* > 0$, magnetic mirrors result[62]. Ideally, these completely reflect the light but with a different phase shift compared with that of ordinary metal mirrors (for which $\mu_r = 1$ and $\varepsilon_r < 0$).

Cross couplings. In the discussion thus far, we have tacitly neglected chiral effects. Macroscopically, chiral effects, such as optical activity, can be described by the dimensionless chirality parameter $\xi(\omega)$[63,64], where ω is the angular frequency of the light. Microscopically, magnetic dipole moments are excited by the electric component of the electromagnetic light wave and vice versa. In the general anisotropic case, these so-called cross terms are referred to as bi-anisotropy[63,64]. Analogous couplings in Eringen continuum mechanics[65] are described below. These cross terms can be non-zero only if space-inversion symmetry or time-inversion symmetry is broken. For light impinging under normal incidence onto a planar 2D system and emerging from it along the same axis, chiral effects are zero by symmetry[66]. Therefore, 3D metamaterials are of particular interest here.

As mentioned at the beginning of this section, chirality enables negative refractive indices via the relation $n_\pm^* = \sqrt{\varepsilon_r^* \mu_r^*} \pm \xi^*$. Here, + refers to right-handed circular polarization and – refers to left-handed circular polarization, respectively. More interestingly, chiral 3D metamaterials can exhibit optical activity many orders of magnitude larger than what is found in natural substances. Furthermore, the wave impedance and the absorption coefficient also depend on the handedness of the circularly polarized light eigenstates. This makes it possible to realize circular polarizers[67], which are materials that transmit one circular polarization of light and that reflect and/or absorb the opposite handedness nearly completely. 3D helical metallic metamaterials (FIG. 2d,e) approach this ideal and even work over one to two octaves of bandwidth[68–70].

Recently, the concept of 3D metamaterials with maximum electromagnetic chirality was introduced[71]. Such media do not interact with one handedness of light impinging from vacuum or air at all, regardless of the incident direction, whereas they interact with the opposite one. This property is intimately connected to duality[71], the condition in which the tensors obey $\varepsilon_r^* = \mu_r^*$. 3D metamaterials with maximum electromagnetic chirality have potential applications in angle-insensitive, helicity-filtering glasses in stereoscopic 3D projection systems and in the optical sensing of chiral molecules[71,72]. Such metamaterials can potentially be built exclusively from dielectric constituents. In essence, the ohmic current in metals is replaced by the displacement current in dielectrics, leading to low losses.

If the excitation of magnetic dipoles by the electric field of light is not symmetric with respect to the excitation of electric dipoles by the magnetic field, the medium breaks time-reversal symmetry, becomes Faraday active and behaves non-reciprocally. For a linear lossless stationary passive medium, this symmetry breaking requires an internal or external static magnetic field. As one consequence, the transmission of light in one direction is no longer equal to the transmission in the opposite direction. Materials with such behaviour have potential for applications. For example, the bulky optical isolators in telecommunication systems are cost drivers, and improved Faraday active metamaterials

2D Huygens metasurfaces
2D arrangements of electric and magnetic polarizable elements that modify the transmitted light yet lead to zero reflections.

Faraday active
Refers to media that rotate the polarization axis of linearly polarized light in the presence of a static magnetic field but that do not change the sense of rotation upon back-reflection of light.

would be highly welcome. Interesting steps in this direction have been taken[73]. This effect must not be confused with asymmetric polarization conversion, which is misleadingly sometimes referred to as asymmetric transmission[74]. We come back to other options of breaking time-reversal symmetry in time-dependent and nonlinear media below.

Finally, obtaining any linear material response requires electric and magnetic moments of higher order than that of dipoles. Toroidal moments have been discussed as a new multipole family for 3D optical metamaterials[75,76]. However, in 2017, it was proved mathematically[77] that electric and magnetic multipole moments are sufficient to describe all possible metamaterial properties, which means that toroidal moments are not needed at this point.

Nonlinearities. The combination of resonances, local field enhancements and local symmetry breaking has raised hopes for new, nonlinear optical 3D metamaterials[78–80] and electro-optic 3D metamaterials[81,82] that are highly efficient. Indeed, new geometries and record-high nonlinear optical susceptibilities have been reported[80], especially for the nonlinear refractive index $n_2^\star$ of metamaterials with $\varepsilon_r^\star \approx 0$ and hence linear refractive index $n^\star \approx 0$ (REF.[80]). However, it has also been pointed out[83] that 3D metamaterials and theoretical blueprints for them have not improved compared with established nonlinear optical crystalline materials in regard to the figure of merit, that is, the accessible phase shift per absorption length or the accessible frequency-conversion efficiency per absorption length. Again, as for negative-index metamaterials, losses inherited from metallic ingredients are responsible[83]. Purely dielectric 3D metamaterials[80,84,85] generally exhibit less-pronounced enhancements but might turn out to be more useful in practice[86].

Acoustic and mechanical metamaterials

We start our discussion of acoustic metamaterials (FIG. 3) with the conceptually simplest case of airborne (or waterborne) acoustics. For acoustic waves in isotropic continua, the compressibility κ is mathematically analogous to the electric permittivity ε_r, and the mass density ρ is analogous to the magnetic permeability μ_r (REF.[87]). Therefore, negative refractive indices can be obtained in acoustics in analogy to optics[88–91]. For example, a negative mass density at finite angular driving frequency ω can be achieved slightly above a mass-and-spring resonance, in which the instantaneous acceleration and force are 180 degrees out of phase[92] (FIG. 3a). Taking different springs in the three spatial directions, the simple scalar mass density ρ can turn into a frequency-dependent mass density second-order tensor $\rho(\omega)^\star$ (REFS[93,94]). 3D blueprints for such metamaterials exploiting this freedom[95,96] have been suggested theoretically[97]. Independent adjustment of the magnitudes of scalar $B(\omega)$ and $\rho(\omega)$ also enables acoustic impedance matching (analogous to optics, as described above). Combined with finite absorption, perfect acoustic absorbers exhibiting zero reflection and zero transmission become possible[91]. For a single Lorentzian resonance, absorption can be close to 100% only over a limited frequency range. However, by using a clever distribution of folded Fabry–Pérot resonators with different resonance frequencies in each unit cell, close to 100% absorption has been obtained experimentally over more than 2 octaves of frequency, from 500 Hz to 3,000 Hz (REF.[98]). The absorber thickness of approximately 11 cm is close to the fundamental limit determined by causality. Some of the authors of REF.[98] have commercialized these 3D metamaterials for applications in noise reduction.

In acoustics, in contrast to optics, it is not trivial to obtain, under meaningful conditions, off-resonant positive refractive indices that are moderately large[99]. Most solid materials have an acoustic impedance that is orders of magnitude larger than the impedance of air, and, therefore, close to 100% of the acoustic wave is reflected at the interface. Under such conditions, the phase velocity in the medium becomes irrelevant. However, labyrinthine metamaterials[100,101] (FIG. 3b) can approximately match the acoustic impedance of air. Simultaneously, the metamaterials slow the phase velocity of the wave by providing a winding detour by labyrinthine channels for sound inside of the unit cell bounded by rigid walls, on a scale much smaller than the acoustic wavelength. Experiments have been reported for 2D[102,103] and 3D[101,104] metamaterials.

An interesting twist that has no counterpart in electromagnetism is that the background air can also be actively driven in the channels of an acoustic metamaterial. This motion breaks reciprocity for a pressure wave propagating in moving air. Metamaterials based on unit cells in which the air is locally circulating, driven by fans, have been demonstrated[105]. By constrictions in the channels, which locally modify the fluid motion, gain and loss regions can be mimicked[106]. On this basis, metamaterials that are symmetric with respect to simultaneous space-inversion and time-inversion (parity-time (PT)-symmetric metamaterials) can be constructed[106].

Cauchy elasticity. The generalization of the 1D Hooke's law to 3D solids led Cauchy to his elasticity tensor C, which connects stresses and strains[107]. The rank-4 Cauchy elasticity tensor is much richer than the rank-2 electric permittivity tensor in optics. In a homogeneous, isotropic medium, the permittivity tensor reduces to a scalar, whereas the elasticity tensor does not. However, the elasticity tensor can be parameterized by two scalars. This can be done, for example, by using the bulk modulus B, equal to the inverse of the compressibility κ, and the shear modulus G. Alternatively, one can use the Young's modulus E and the Poisson ratio ν or other combinations[107]. In an unconstrained stable passive medium under stationary conditions ($\omega = 0$), B and G cannot be negative. Likewise, Hooke's spring constant cannot be negative. The bounds on other elastic parameters, such as E, ν or the Lamé parameters, follow from that constraint[108]. Intuitively, the difference in the rank of the tensors is connected to the fact that electromagnetism usually supports only transverse waves, whereas elasticity generally supports transverse and longitudinal waves simultaneously. For the special case of acoustics, with air or water as the medium, only the longitudinal pressure waves remain because the shear modulus is zero.

Cauchy elasticity tensor
This tensor is the generalization of Hooke's spring constant. It connects the stress and the strain tensors.

Lamé parameters
A possible pair of parameters that characterize the Cauchy elasticity tensor in an isotropic homogeneous medium. The second Lamé parameter is identical to the shear modulus.

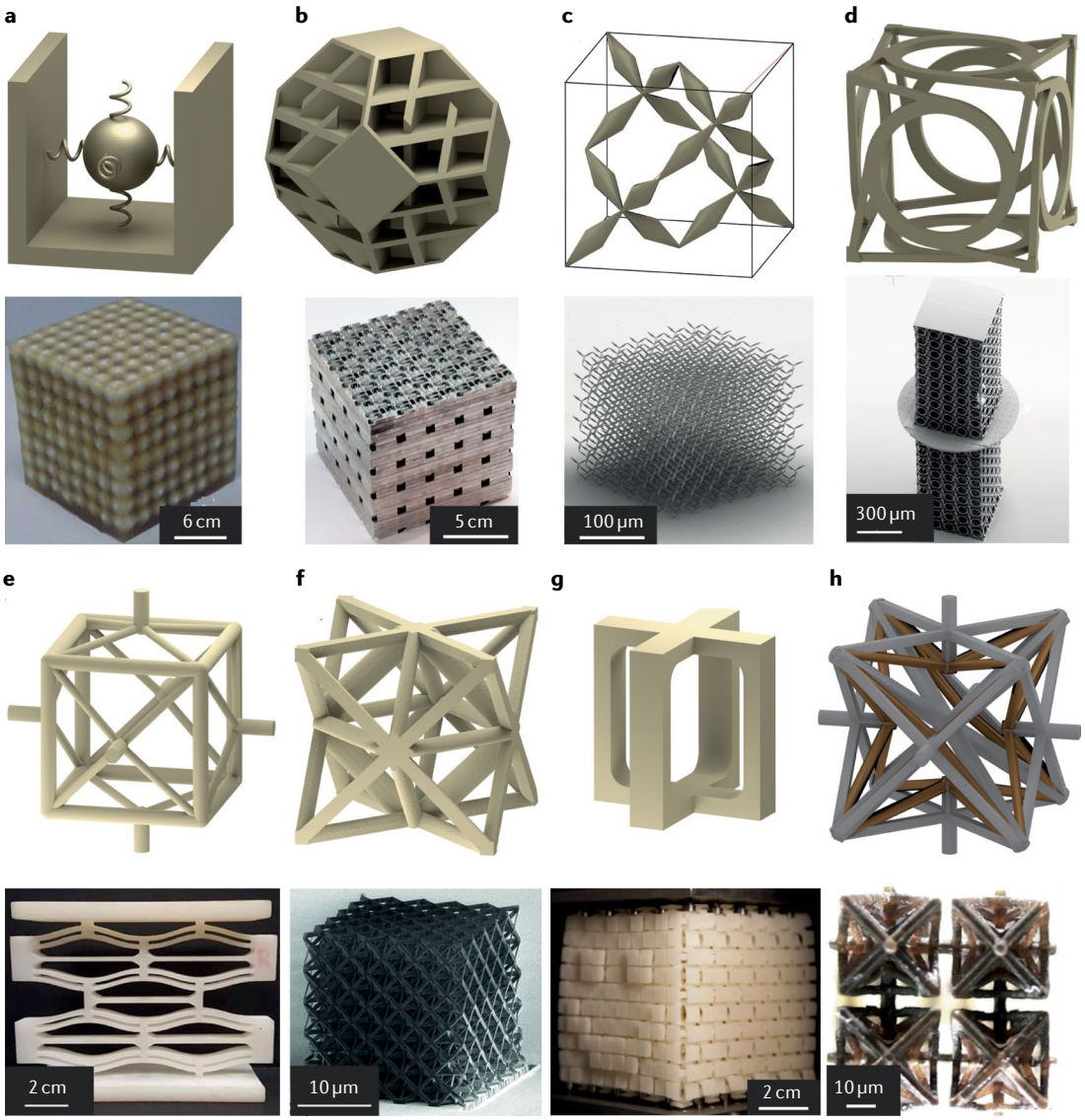

Fig. 3 | **Gallery of designed 3D acoustical and mechanical metamaterial unit cells and corresponding experimental realizations. a** | Unit cell with internal mass–spring resonance that leads to negative effective mass density. **b** | 3D labyrinthine channel system that leads to an isotropic slowing down of sound propagation. **c** | Pentamode cell that gives rise to a small shear modulus (compared with the auxetic cell in FIG. 1d, which leads to a small bulk modulus). **d** | 3D chiral mechanical metamaterial. **e** | Buckling elements that lead to multistable and programmable behaviour. **f** | Truss lattices with a large coordination number leading to strong ultralight behaviour. **g** | Unit cell for a programmable mechanical metamaterial. When the top of the resulting structure, which is composed of many different cells, is pressed, a programmed smiley face appears. **h** | Two-component cell supporting sign reversal of thermal expansion. Panels **a**–**g** show unit cells used in mechanical and acoustic metamaterials; panel **h** shows a unit cell used for stimuli-responsive behaviour. The lower part of panel **a** is adapted with permission from REF.[92], AAAS. Panel **b** is adapted from REF.[101], Frenzel, T. et al. Three-dimensional labyrinthine acoustic metamaterials. *Appl. Phys. Lett.* **103**, 061907 (2013), with the permission of AIP Publishing. Panel **c** is adapted from REF.[111], Kadic, M. et al. On the practicability of pentamode mechanical metamaterials. *Appl. Phys. Lett.* **100**, 19101 (2012), with the permission of AIP Publishing. Panel **d** is adapted with permission from REF.[121], AAAS. Panel **e** is adapted with permission from REF.[194], Emerald Publishing Limited. Panel **f** is adapted with permission from REF.[151], AAAS. Panel **g** is adapted from REF.[142], Springer Nature Limited. Panel **h** is adapted with permission from REF.[195], APS.

For elastic solids, unlike air or water, the shear modulus G is generally not zero. In auxetic elastic metamaterials, the effective shear modulus G^* can even be made larger than the effective bulk modulus B^*. Equivalently, the effective Poisson ratio ν^* is negative. Such materials contract laterally when pushed on (FIG. 1d). For 3D isotropic dilational metamaterials, in the limit $G^* \gg B^*$, the Poisson ratio tends to −1, which means that the softest mode of material deformation is a change in volume without a change in shape of the material[109]. Thus, applications in shock protection by stress distribution are envisioned[109].

The opposite limit of $G^* \ll B^*$ is that of pentamode metamaterials[110] (FIG. 3c), which behave approximately as liquids with $G = 0$; hence, $\nu = 0.5$. 3D pentamodes[111] and anisotropic versions thereof[112] have been realized

experimentally. Loosely speaking, pentamode metamaterials are more rubbery than rubber in the sense that the effective B/G ratio can exceed 10^3. The soles composed of microlattices in the 3D printed shoes of a major sports manufacturer are related to this idea. Notably, the two limits of $\nu^* \to -1$ and $\nu^* \to +0.5$ are the only cases for which a cubic-symmetry 3D periodic metamaterial can generally be described by an isotropic Poisson ratio[113]. Conceptually, all conceivable 3D Cauchy elasticity tensors can be constructed from pentamode materials[110].

Poroelastic metamaterials[114–116] combine much of what has been discussed above. In their elastic constituent solid, they support phonons, and in their voids, which are filled with air or a fluid, they support acoustic waves. If these waves are phase matched, they can form mixed elastic–acoustic modes[17]. In the static regime, 3D cubic poroelastic metamaterials containing hollow inner volumes sealed by thin membranes have led to a negative static effective compressibility, even though both constituents, air and solid, have positive compressibility[116–118]. This means that the effective volume enclosed by the metamaterial surfaces increases when the surrounding hydrostatic air pressure increases. Because the effective volume $V_{\text{eff}} = Na^3$ of N unit cells is not a thermodynamic quantity, this highly unusual sign reversal does not violate any law of physics.

Generalized elasticity. For linear optical metamaterials, our discussion opened with the observation that most optics textbooks deal with only the electric permittivity tensor ε_r of continua and neglect magnetism at optical frequencies. For linear elastic mechanical materials, the situation is similar. Most standard textbooks[119] describe elastic continua on the level of Cauchy elasticity using the elasticity tensor C, which connects stresses and strains[107] but neglects rotations. Again, the lattice constant a is a determining factor. If the lattice constant a is small compared with all other relevant spatial scales, namely, wavelength and sample size, Cauchy elasticity is sufficient. This is analogous to the fact that the electric permittivity is sufficient for electromagnetic continua in the limit $a \to 0$, as described in the section on electromagnetic and optical metamaterials. The reason is that the rotation of a point-like object has no meaning. Therefore, electric fields in optics and displacements in mechanics are analogous. For intermediate metamaterial lattice constants, however, an additional rotational field generally becomes important[65,120]. This rotational field is analogous to the magnetic field of the light in optics. The analogy between optics and mechanics continues in that cross terms — couplings between displacements and rotations — can occur for 3D chiral mechanical metamaterials[121,122].

Whereas all these aspects are elements of Eringen micropolar continuum mechanics[65], they have only recently become experimental reality in the field of metamaterials[121,122] (FIG. 3d). In 3D chiral mechanical metamaterials, a pronounced conversion of a static axial push onto a beam into a twist of the beam was observed. This twist, which is forbidden in Cauchy elasticity, decayed only slowly with increasing number of unit cells in the beam[121,122]. Some say that scalability is lost, because the properties depend on the size of the material and not only on the material itself. This notion has to be taken with some caution: although certain behaviour does depend on the number of unit cells in the metamaterial, the entries in the effective generalized Eringen elasticity tensors do not depend on size. The up-to-12 independent moduli for cubic 3D micropolar metamaterials (196 for triclinic) are bound in a complex way by reciprocity and the requirement that the eigenvalues cannot be negative[107]. In the dynamic case, 3D chiral phonons result[123]. In achiral 2D and 3D metamaterials, a related behaviour was found[124]. There, for example, the effective static Hooke's spring constant does not double if one cuts a metamaterial beam in half[124]. A characteristic length scale, which depends on the geometry of the metamaterial unit cell, can tend to infinity, meaning that Cauchy elasticity is not recovered even for large samples[124,125].

Recent theoretical work has gone one step further and considered gyroelastic metamaterials[5,126–128], which are the counterpart of Faraday active metamaterials in optics. A built-in continuously rotating gyroscope replaces the static magnetic field required in optics. In this way, the mechanical metamaterial unit cell breaks not only space-inversion symmetry via chirality but also time-inversion symmetry. This leads to an asymmetric cross coupling between torques and displacements on the one hand and between forces and rotations on the other hand[65,120] (see the section on electromagnetic and optical metamaterials for a comparison).

We emphasize, however, that the generalizations of Cauchy elasticity discussed thus far are not the only possible ones. The rotations in Eringen continuum mechanics are, in a way, perturbations to regular elasticity. By contrast, in strain-gradient metamaterials[129], some components of the effective elasticity tensor are zero, and the main contribution is the strain gradient term[130–135]. As for chiral metamaterials, Cauchy elasticity is not recovered in the large-sample limit. Another generalization is Willis metamaterials[94], for which stress in the dynamic case depends on acceleration and not only strain, and momentum depends on the displacement gradient and not only velocity.

Nonlinearities. Thus far, we have focused on linear mechanics. However, nonlinearities play a tremendous role in engineering. We distinguish between reversibly nonlinear mechanical behaviour, such as buckling instabilities[136–138], and irreversibly nonlinear behaviour, such as failure or fracture of the constituent material or materials.

Whereas reversible nonlinearities are often only a minor correction to the linear behaviour in optics, geometrical nonlinearities can have very large effects in mechanics, even if the constituent material behaves perfectly linearly. The nonlinearities can be tailored by the metamaterial unit cell geometry. It has been proved by construction that essentially any nonlinear mechanical behaviour can be achieved[109,139,140]. Even multistable behaviour is possible, on the basis of the buckling of beams. This classic mechanism is closely related to the 'click' you hear when pushing onto the lid

Eringen micropolar continuum mechanics
A generalization of Cauchy continuum mechanics, in which four rank-4 tensors are required to describe the connection between strain and microrotation tensors and between stress and torque tensors.

of a marmalade jar. Beyond a certain strain, the stress no longer increases but rather decreases. Assembling a 3D metamaterial (FIG. 3e) out of such buckling beams, in parallel and in serial, couples them. Under strain control, the resulting behaviour is nonlocal. The buckling of one beam influences beams far away, because the displacements of all unit cells have to add up to the prescribed overall displacement. The resulting stress–strain behaviour is multistable[137,138,141]. Upon loading and unloading such a metamaterial, it does not follow the same path in stress–strain space. This means that energy is irreversibly dissipated as heat during each cycle. As the constituent material can be purely linearly elastic in this process, the cycling is repeatable many times. Applications in terms of shock absorbers have been suggested[141]. The buckling beams can also be designed to be multistable by themselves. In this case, the 3D metamaterial has multiple stable states at zero external force. The different states generally have different linear elastic behaviour[142]. Therefore, the elastic behaviour can be programmed in this sense (see also origami metamaterials[143–146]). Finally, in the nonlinear regime, such as for a buckling metamaterial, the stress–strain curve $\sigma(\varepsilon)$ does not need to be symmetric with respect to pushing or pulling, that is, it is possible for $\sigma(-\varepsilon) \neq -\sigma(\varepsilon)$. This asymmetry in the nonlinear response for a 1D 'fishbone' metamaterial has been interpreted in terms of static non-reciprocity[147]. By sharp contrast, in the linear elastic regime, the stress–strain curve for passive media must obey the condition $\sigma(-\varepsilon) = -\sigma(\varepsilon)$, even for asymmetric structures.

With respect to irreversible mechanical failure and fracture, the idea of 3D lightweight metamaterials has sparked considerable interest[139,148–152]. When decreasing the volume filling fraction f of the constituent material, the effective mass density $\rho^\star$ decreases proportionally. At the same time, the stiffness and the strength, that is, the stress σ at failure, also decrease unavoidably. However, the scaling exponent η between effective strength $\sigma^\star$ and mass density, $\sigma^\star \propto (\rho^\star)^\eta$, can be influenced by the 3D metamaterial architecture[149,150,153]. The value of η depends on whether the behaviour is dominated by beam bending or stretching. Truss-based lattices with a large coordination number (or structural connectivity) turn out to be favourable for achieving large strength[153] (FIG. 3f). Along these lines, 3D microlattices approaching the maximum possible theoretical strength have been achieved[149,150,152]. None of these metamaterials is scalable, in the sense that their properties change if all unit cell dimensions are scaled down by the same factor. To avoid confusion, we emphasize that loss of scalability in the sense used here is distinct from that mentioned in the context of the micropolar 3D metamaterials discussed above.

Transport metamaterials

Because they are response functions, simple transport coefficients such as the electrical conductivity σ, the diffusivity D and the thermal conductivity κ of passive materials cannot be negative under stationary conditions, that is, when $\omega = 0$, owing to energy conservation and the second law of thermodynamics. The specific heat c of a stable material cannot be negative either. Therefore, parameter sign reversals of these quantities in analogy to the refractive index are not allowed. However, this rule does not apply to active metamaterials, as discussed below.

Other stationary transport coefficients such as the Hall coefficient[154–156] A_H, the Ettingshausen coefficient P_E, the Seebeck coefficient S, the Peltier coefficient Π and the relative magnetoresistance change $\Delta R/R$ can be positive or negative in the stationary regime[157]. Although obtaining non-reciprocal behaviour is a hot and demanding topic in optics, acoustics and mechanics, it is standard in transport owing to the existence of semiconductor p–n diodes.

Additional bounds apply for composites. The isotropic Hall coefficient $A_H^\star$ of a 2D metamaterial in a perpendicular magnetic field cannot have the opposite sign of the isotropic Hall coefficients of its constituents[155]. The same holds for 3D hierarchical laminates[5]. In 3D structures beyond laminates, this restriction does not apply, and parameter sign reversal is allowed[156,158,159]. The same analogously applies to the Ettingshausen coefficient P_E. For Hall-effect-based magnetic field sensors, which are used, for instance, in the compass apps of many modern mobile phones, the modulus of the Hall mobility μ_H, which is given by the product $\mu_H = A_H\sigma$, determines the sensitivity and the signal-to-noise ratio of the sensor. In a metamaterial made of non-magnetic constituents, the effective isotropic Hall mobility $\mu_H^\star$ is fundamentally bounded by twice the largest Hall mobility of the constituents[160]. This bound can be broken in the presence of additional tailored spatial distributions of static paramagnetic and diamagnetic constituents within the composite[160].

The commonly used figure of merit for devices aiming at efficient thermoelectric energy conversion is the dimensionless non-negative ZT value. This value is given by $ZT = \sigma S^2 T/\kappa$, where T is the thermodynamic temperature[161]. It has been shown theoretically that for an arbitrary composite in a small or zero magnetic field, the effective $ZT^\star$ value cannot exceed the largest ZT value of its constituents[161]. However, this technologically unfortunate bound can be broken in the presence of large magnetic fields[161,162] (FIG. 4a with material replaced by voids and vice versa). Furthermore, at least one of the constituents of the metamaterial must have a strong thermoelectric response, and another constituent must have a strong Hall effect, that is, a large Hall mobility. It has been argued, though, that the power factor (that is, conversion capacity) may be equally important technologically[163]. Power factors of thermoelectric materials, unlike the figure of merit, can be improved by orders of magnitude using metamaterials, for instance, by lamination (FIG. 2c) of two or more thermoelectric constituent materials.

Transport experiments. In analogy to the situations in optics and mechanics, passive laminates or laminates of laminates (FIG. 4b) have led to anisotropic electrical, thermal and diffusive transport, using isotropic constituent materials[5,164], as well as to improved thermoelectric power factors[163].

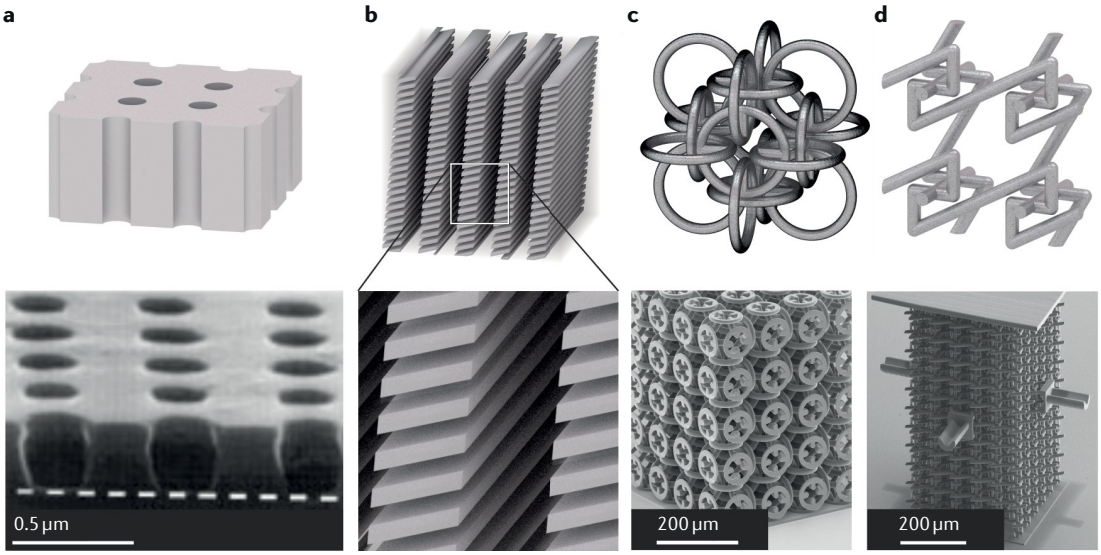

Fig. 4 | **Gallery of designed transport metamaterial unit cells and corresponding experimental realizations.** **a** | Square array of cylindrical holes in a plate, leading to anisotropic, indefinite or hyperbolic behaviour. **b** | A hierarchical laminate (also known as a Maxwell laminate). **c** | A chainmail-like arrangement of tori leading to sign reversal of the isotropic Hall coefficient. **d** | An anisotropic cell supporting the parallel Hall effect. Panel **a** is adapted with permission from REF.[157], APS. Panel **c** is adapted with permission from REF.[159], APS. Panel **d** is adapted with permission from REF.[166], APS.

Absolute negative mobility has been shown in active 2D microfluidic systems[165], following an earlier theoretical suggestion. There, micrometre-sized polystyrene beads always moved in a direction opposite to that of the net acting force as a result of an interplay between thermal noise, the periodic and symmetric microfluidic structure and a biased alternating current (AC) electric field[165].

Effective classical magnetoresistance that is highly anisotropic has been demonstrated in passive microstructures composed of Hall bars made out of a 3D layer of n-type GaAs, punctured by a square array of cylindrical voids in the *xy*-plane[157] (FIG. 4a). The modulus of the effective magnetoresistance at $T = 90$ K was found to be as large as $\Delta R^{*}_{xx} / R^{*}_{xx} \approx 65\%$ at an in-plane magnetic field corresponding to $B_y = 12$ T (REF.[157]). By sharp contrast, the constituent GaAs crystal showed essentially zero magnetoresistance. This work follows from preceding theoretical work[157]. In the strict 2D limit of a thin platelet, the magnetoresistance tends to zero theoretically[154]. Intuitively, the origin of the metamaterial magnetoresistance was interpreted in terms of a 'geometrical shadow' of the current along the direction of the magnetic field, which is cast by the voids in the semiconductor[157].

A sign reversal of the effective 3D isotropic Hall coefficient with respect to the n-type ZnO constituent material has been observed[159] at room temperature in cubic-symmetry chainmail-like metamaterials (FIG. 4c), composed of interlinked hollow tori. This sign reversal was previously predicted theoretically[155,156,158]. The origin of this sign reversal can be traced back to the different topologies of a bulk material and a (hollow) torus made out of it[159]. Two additional distinct paths to a sign reversal of A^{*}_{H} in 3D have been suggested theoretically[160]. One is based on exchanging the pick-up leads, and the other on reversing the local direction of the magnetic field, both in cubic symmetry. In lower-symmetry metamaterials (FIG. 2d), off-diagonal components of the Hall tensor can dominate over the diagonal components[160]. Experiments on 3D metamaterials have shown the resulting unusual Hall voltage to be parallel, rather than perpendicular, to the external magnetic field[166] (FIG. 4d). The parallel Hall effect could be used for sensors measuring the local circulation of a magnetic field[166]. It appears that any Hall tensor that is compatible with the Onsager relations[167] can be realized by 3D metamaterials composed of isotropic constituents[160]. However, a constructive proof for this conjecture is absent to date.

Stimuli-responsive metamaterials

The properties and associated effective-medium parameters of metamaterials are not necessarily fixed: they can be influenced by external stimuli and thereby be changed deterministically with time. Such behaviour requires that the constituent materials respond to some sort of stimulus, such as the light intensity, electric field, magnetic field, pressure or temperature. Liquid crystal displays are a widespread example, in which the optical properties are changed by the application of electric fields that locally modulate the local liquid crystal orientation in each pixel. Using light as the stimulus for transparent metamaterials allows selective addressing of individual unit cells in three dimensions, which tends to be difficult for other stimuli. 3D stimuli-responsive constituent materials are an active field of research in their own right[168–177]. Ideally, the metamaterial unit cell leverages these changes in some way, for example, by resonances or geometrical nonlinearities. Provided the metamaterial is multistable, the stimulus can even programme the metamaterial, in the sense that the reversibly induced change persists after the stimulus is switched off. FIGURE 3g gives an example of a programmable metamaterial, and FIG. 3h of a stimuli-responsive

Table 1 | **Exemplary publications on stimuli-responsive metamaterials**

	Optical/ electromagnetic response	Mechanical/acoustical response	Transport properties
Electromagnetic stimulus	REFS[196–199]	REFS[200,201]	REFS[200,202]
Mechanical stimulus	REFS[203,204]	REFS[142,205]	REF.[206]
Thermodynamic stimulus	REFS[202,207,208]	REFS[177,209–211] (see FIG. 3h)	REF.[212]

metamaterial. TABLE 1 provides an overview of literature on the experimental status of stimuli-responsive and programmable metamaterials, albeit not all in 3D. The columns refer to different material properties, the rows refer to different types of stimuli. The upper two elements on the diagonal are the same as nonlinear optics and nonlinear mechanics, respectively.

Stimulating all unit cells of a 3D metamaterial in the same way leads to tuneable metamaterials, which could find applications as modulators. The metamaterial unit cells can be the same initially and then change in different ways, thereby inducing specific functionality by a stimulus[178–183]. Moreover, the time-dependent stimulation can be such that it creates a circulation of some property within one metamaterial unit cell. The axis associated with this circulation acts analogously to a static magnetic field in Faraday active optical materials and can thus lead to non-reciprocal propagation of electromagnetic[184] or acoustic waves[105] in 2D metamaterial lattices made out of 3D unit cells.

In addition, the properties can vary not only in space but also in time. Rather than having a unit cell of periodicity in space, the metamaterial has a unit cell of periodicity in 4D space–time[175,185,186]. Modulation of material properties in time can be achieved by external stimuli, as discussed above. Many unusual behaviours are theoretically predicted in space–time metamaterials, although it should be emphasized that theory, thus far, has focused on only one spatial dimension plus time. One predicted behaviour is that when waves are reflected off the interface of space–time metamaterials at rest in the laboratory frame, the metamaterials can mimic the Doppler frequency shift that occurs for media moving in the laboratory frame[187]. Another theoretical proposal is the use of artificial magnetic fields for photons with an artificial Lorentz effect so that the photons travel along circular arcs[188]. Tilted band structures are proposed to provide unidirectional bandgaps[189]. Furthermore, striking new types of wave behaviour, called field patterns[190], are theoretically predicted. The material wave and the propagating wave are concentrated on a pattern, that is, the field pattern. Macroscopically, the wave amplitude blows up exponentially if PT symmetry is broken or remains bounded if PT symmetry is unbroken. In the unbroken case, the wake behind a wavefront does not die away, and instead the material remains excited.

Thus far, however, the concept of space–time metamaterials is theoretical[191]. Experiments need to identify suitable stimuli-responsive mechanisms (TABLE 1) with sufficiently small response times and corresponding constituent materials, enabling such architectures to be manufactured.

Conclusions and perspectives

Although there has been a lot of interest in metamaterials research in the past two decades, we should humbly admit that not all new ideas are good and that not all good ideas are new. More than a century ago, Maxwell discussed laminates that provide an anisotropic response from isotropic ingredients. In 1920, Lindman investigated arrangements of metal helices that lead to a giant effective chiral response (optical activity) from achiral ingredients. Some of the history has been described[5]. However, at least three things have changed since Maxwell and Lindman. The rise of nanotechnology has enabled the manufacture of optical metamaterials, composed of unit cells with sub-wavelength feature sizes. Furthermore, reliable 3D additive manufacturing (or, loosely, 3D printing) on various spatial scales has enabled the fabrication of complex 3D architectures for electromagnetism, optics, acoustics, mechanics and transport that seemed very difficult if not impossible to make 20 years ago. In parallel, substantial progress has been made and new approaches developed in theoretical design efforts, which could build on substantial advances in numerical computation and inverse design.

Metamaterials researchers can be proud. A long-standing dream of condensed matter physics is to design materials on the computer, to avoid tedious trial-and-error procedures and excessive experimentation. However, the truth is that this dream has been realized in only a few exceptional cases to date. Metamaterials are an entire class of such exceptions. A wide variety of highly unusual 3D metamaterial properties has been creatively predicted and then confirmed experimentally.

Let us finally speculate about possible future perspectives of the field. At present, the number of researchers working on 2D metasurfaces is much larger than the number working on 3D metamaterials. It is argued that 2D structures are easier to fabricate, bringing the field closer to applications. Flat electromagnetic and optical metalenses are a prominent example. However, recent advanced meta-lenses use two or more layers to obtain additional degrees of freedom in the design process, in analogy to ordinary refractive-lens systems; otherwise, certain aberrations simply cannot be corrected. This means that the 2D metasurface field is partly moving to 3D architectures. This step is not surprising in view of the fact that, conceptually, the possibilities of 2D structures are only a subset of the possibilities of 3D structures. Furthermore, with the rapid progress of 3D additive manufacturing, in future years, 3D structures might be as easy to manufacture as 2D structures are today.

The connection between 3D metamaterials and 3D additive manufacturing might become even tighter. A dream is to be able to 3D print anything, including functional devices. Gaining this ability will require realizing thousands of different optical, magnetic, mechanical and transport material properties. Thousands of different input material cartridges are unlikely to be

a viable solution. Today's 2D graphical inkjet printers achieve thousands of different colours by mixing the inks from only three colour cartridges. By analogy, on the basis of microstructure rather than mixing, future 3D material printers may achieve thousands of different effective metamaterial properties starting from only a small number of input material cartridges. This Review has illustrated many steps in this direction.

Published online 31 January 2019

1. Walser, R. M. Electromagnetic metamaterials. *Proc. SPIE, Complex Mediums II: Beyond Linear Isotropic Dielectr.* (eds Lakhtakia, A., Weiglhofer, W. S. & Hodgkinson, I. J.) **4467** (2001).
2. Bendsøe, M. & Sigmund, O. *Topology Optimization: Theory, Methods and Applications* (Springer, 2004).
3. Browning, V. *DARPATech 2002* **7**, 791–795 (2002).
4. Kittel, C. *Introduction to Solid State Physics* (Wiley, 2004).
5. Milton, G. W. *The Theory of Composites* (Cambridge Univ. Press, 2002).
This textbook provides a comprehensive theoretical introduction to man-made composite materials in electromagnetism and optics, acoustics and mechanics, and transport.
6. Golden, K., Grimmett, G., James, R., Milton, G. & Sen, P. *Mathematics of Multiscale Materials* (Springer, New York, 2012).
7. Chen, H.-T., Taylor, A. J. & Yu, N. A review of metasurfaces: physics and applications. *Rep. Prog. Phys.* **79**, 076401 (2016).
8. McCall, M. et al. Roadmap on transformation optics. *J. Opt.* **20**, 063001 (2018).
9. Craster, R. V., Kaplunov, J. & Pichugin, A. V. High-frequency homogenization for periodic media. *Proc. R. Soc. Lond. Ser. A* **466**, 2341–2362 (2010).
10. Bensoussan, A., Lions, J. & Papanicolaou, G. *Asymptotic Analysis for Periodic Structures* (American Mathematical Society, 2011).
11. Jikov, V., Yosifian, G., Kozlov, S. & Oleinik, O. *Homogenization of Differential Operators and Integral Functionals* (Springer, Berlin Heidelberg, 2012).
12. Bakhvalov, N. & Panasenko, G. *Homogenisation: Averaging Processes in Periodic Media: Mathematical Problems in the Mechanics of Composite Materials* (Springer, Netherlands, 2012).
13. Pham, K., Maurel, A. & Marigo, J.-J. Two scale homogenization of a row of locally resonant inclusions — the case of anti-plane shear waves. *J. Mech. Phy. Solids* **106**, 80–94 (2017).
14. Brassart, M. & Lenczner, M. A two-scale model for the periodic homogenization of the wave equation. *J. Math. Pures Appl.* **93**, 474–517 (2010).
15. Harutyunyan, D., Milton, G. W. & Craster, R. V. High-frequency homogenization for travelling waves in periodic media. *Proc. R. Soc. Lond. Ser. A* **472**, 20160066 (2016).
16. Krushlov, E. Y. The asymptotic behavior of solutions of the second boundary value problem under fragmentation of the boundary of the domain. *Math. USSR Sb.* **35**, 266–282 (1979).
17. Auriault, J. L. & Boutin, C. Deformable porous media with double porosity III: acoustics. *Transp. Porous Med.* **14**, 143–162 (1994).
18. Zhikov, V. V. On an extension of the method of two-scale convergence and its applications. *Sb. Math.* **191**, 31–72 (2010).
19. Pendry, J. B., Holden, A. J., Stewart, W. J. & Youngs, I. Extremely low frequency plasmons in metallic mesostructures. *Phys. Rev. Lett.* **76**, 4773–4776 (1996).
20. Belov, P. A. et al. Strong spatial dispersion in wire media in the very large wavelength limit. *Phys. Rev. B* **67**, 113103 (2003).
21. Menzel, C. et al. Validity of effective material parameters for optical fishnet metamaterials. *Phys. Rev. B* **81**, 035320 (2010).
22. Soukoulis, C. & Wegener, M. Past achievements and future challenges in the development of three-dimensional photonic metamaterials. *Nat. Photonics* **5**, 523–530 (2011).
This reference is an extensive review on 3D optical metamaterials, with emphasis on negative refractive indices and chirality; it also provides a more detailed history of the field.
23. Laude, V. *Phononic Crystals: Artificial Crystals for Sonic, Acoustic, and Elastic Waves* (De Gruyter, 2015).
This is a textbook introduction to acoustic and elastic metamaterials.
24. Kane, C. L. & Lubensky, T. C. Topological boundary modes in isostatic lattices. *Nat. Phys.* **10**, 39–45 (2014).
25. Süsstrunk, R. & Huber, S. D. Observation of phononic helical edge states in a mechanical topological insulator. *Science* **349**, 47–50 (2015).
26. Süsstrunk, R. & Huber, S. D. Classification of topological phonons in linear mechanical metamaterials. *Proc. Natl Acad. Sci. USA* **113**, E4767–E4775 (2016).
27. Landau, L. D. & Lifshitz, E. M. *Electrodynamics of Continuous Media* (Pergamon Press, 1960).
28. Schelkunoff, S. A. & Friis, H. T. *Antennas: the Theory and Practice* (Wiley, 1952).
29. Pendry, J. B., Holden, A. J., Robbins, D. J. & Stewart, W. J. Magnetism from conductors and enhanced nonlinear phenomena. *IEEE Trans. Microwave Theory Tech.* **47**, 2075–2084 (1999).
30. Schneider, H. J. & Dullenkopf, P. Slotted tube resonator: a new NMR probe head at high observing frequencies. *Rev. Sci. Instrum.* **48**, 68–73 (1977).
31. Ghim, B. T., Rinard, G. A., Quine, R. W., Eaton, S. S. & Eaton, G. R. Design and fabrication of copper-film loop–gap resonators. *J. Magn. Reson. A* **120**, 72–76 (1996).
32. Lagarkov, A. N. & Sarychev, A. K. Electromagnetic properties of composites containing elongated conducting inclusions. *Phys. Rev. B* **53**, 6318–6336 (1996).
33. Rose-Innes, A. & Rhoderick, E. *Introduction to Superconductivity* (Pergamon Press, 1978).
34. Meade, R. & Diffenderfer, R. *Foundations of Electronics: Circuits and Devices* (Delmar Cengage Learning, 2002).
35. Dolling, G., Enkrich, C., Wegener, M., Soukoulis, C. M. & Linden, S. Simultaneous negative phase and group velocity of light in a metamaterial. *Science* **312**, 892–894 (2006).
36. Veselago, V. The electrodnamics of substances with simultaneously negative values of and μ. *Sov. Phys. Usp.* **10**, 509–514 (1968).
This is an inspiring 'what if' paper, showing some of the enhanced possibilities with negative magnetic permeability and negative refractive index in optics; it stimulates much of the early work on electromagnetic and optical metamaterials.
37. Pendry, J. B. Negative refraction makes a perfect lens. *Phys. Rev. Lett.* **85**, 3966–3969 (2000).
38. Shelby, R. A., Smith, D. R. & Schultz, S. Experimental verification of a negative index of refraction. *Science* **292**, 77–79 (2001).
This experimental paper on negative refractive indices at microwave frequencies is a catalyser for the metamaterial field.
39. Zhang, S. et al. Experimental demonstration of near-infrared negative-index metamaterials. *Phys. Rev. Lett.* **95**, 137404 (2005).
40. Soukoulis, C. M., Linden, S. & Wegener, M. Negative refractive index at optical wavelengths. *Science* **315**, 47–49 (2007).
41. García-Meca, C. et al. Low-loss multilayered metamaterial exhibiting a negative index of refraction at visible wavelengths. *Phys. Rev. Lett.* **106**, 067402 (2011).
42. Kinsler, P. & McCall, M. W. Causality-based criteria for a negative refractive index must be used with care. *Phys. Rev. Lett.* **101**, 167401 (2008).
43. Zheludev, N. I., Prosvirnin, S. L., Papasimakis, N. & Fedotov, V. A. Lasing spaser. *Nat. Photonics* **2**, 351–354 (2008).
44. Noginov, M. A. et al. Demonstration of a spaser-based nanolaser. *Nature* **460**, 1110–1112 (2009).
45. Fang, A., Koschny, T., Wegener, M. & Soukoulis, C. M. Self-consistent calculation of metamaterials with gain. *Phys. Rev. B* **79**, 241104 (2009).
46. Wuestner, S., Pusch, A., Tsakmakidis, K. L., Hamm, J. M. & Hess, O. Overcoming losses with gain in a negative refractive index metamaterial. *Phys. Rev. Lett.* **105**, 127401 (2010).
47. Valentine, J. et al. Three-dimensional optical metamaterial with a negative refractive index. *Nature* **455**, 376–379 (2008).
48. Nguyen, V. C., Chen, L. & Halterman, K. Total transmission and total reflection by zero index metamaterials with defects. *Phys. Rev. Lett.* **105**, 233908 (2010).
49. Moitra, P. et al. Realization of an all-dielectric zero-index optical metamaterial. *Nat. Photonics* **7**, 791–795 (2013).
50. Javani, M. H. & Stockman, M. I. Real and imaginary properties of epsilon-near-zero materials. *Phys. Rev. Lett.* **117**, 107404 (2016).
51. Wegener, M., Dolling, G. & Linden, S. Plasmonics: backward waves moving forward. *Nat. Mater.* **6**, 475–476 (2007).
52. Yao, J. et al. Optical negative refraction in bulk metamaterials of nanowires. *Science* **321**, 930 (2008).
53. Cui, T., Smith, D. & Liu, R. *Metamaterials: Theory, Design, and Applications* (Springer, 2009).
54. Krishnamoorthy, H. N., Jacob, Z., Narimanov, E., Kretzschmar, I. & Menon, V. M. Topological transitions in metamaterials. *Science* **336**, 205–209 (2012).
55. García-Chocano, V. M., Christensen, J. & Sánchez-Dehesa, J. Negative refraction and energy funneling by hyperbolic materials: an experimental demonstration in acoustics. *Phys. Rev. Lett.* **112**, 144301 (2014).
56. Ferrari, L., Wu, C., Lepage, D., Zhang, X. & Liu, Z. Hyperbolic metamaterials and their applications. *Prog. Quantum Electron.* **40**, 1–40 (2015).
57. Landy, N. I., Sajuyigbe, S., Mock, J. J., Smith, D. R. & Padilla, W. J. Perfect metamaterial absorber. *Phys. Rev. Lett.* **100**, 207402 (2008).
58. Liu, N. et al. Plasmonic analogue of electromagnetically induced transparency at the drude damping limit. *Nat. Mater.* **8**, 758–762 (2009).
59. Watts, C. M., Xianliang, L. & Padilla, W. J. Metamaterial electromagnetic wave absorbers. *Adv. Mater.* **24**, 98–120 (2012).
60. Lee, Y., Rhee, J., Yoo, Y. & Kim, K. *Metamaterials for Perfect Absorption* (Springer, Singapore, 2016).
61. Pfeiffer, C. & Grbic, A. Metamaterial huygens surfaces: tailoring wave fronts with reflectionless sheets. *Phys. Rev. Lett.* **110**, 197401 (2013).
62. Liu, S. et al. Optical magnetic mirrors without metals. *Optica* **1**, 250–256 (2014).
63. Lindell, I. *Electromagnetic Waves in Chiral and Bi-isotropic Media* (Artech House, 1994).
64. Tretyakov, S., Sihvola, A., Sochava, A. & Simovski, C. Magnetoelectric interactions in bi-anisotropic media. *J. Electro. Wave. Appl.* **12**, 481–497 (1998).
65. Eringen, A. *Elastodynamics* Vol. 2 (Academic Press, 1974).
66. Wegener, M. & Linden, S. in *Tutorials in Metamaterials* Ch. 8 (eds Noginov, M. A. & Podolskiy, V. A.) (Taylor and Francis, 2012).
67. Gansel, J. et al. Gold helix photonic metamaterial as broadband circular polarizer. *Science* **325**, 1513–1515 (2009).
68. Gansel, J. et al. Tapered gold-helix metamaterials as improved circular polarizers. *Appl. Phys. Lett.* **100**, 101109 (2012).
69. Johannes, K. et al. A helical metamaterial for broadband circular polarization conversion. *Adv. Opt. Mater.* **3**, 1411–1417 (2015).
70. Kaschke, J. & Wegener, M. Gold triple-helix mid-infrared metamaterial by sted-inspired laser lithography. *Opt. Lett.* **40**, 3986–3989 (2015).
71. Fernandez-Corbaton, I., Fruhnert, M. & Rockstuhl, C. Objects of maximum electromagnetic chirality. *Phys. Rev. X* **6**, 031013 (2016).
72. Lefier, Y., Salut, R., Suarez, M. A. & Grosjean, T. Directing nanoscale optical flows by coupling photon spin to plasmon extrinsic angular momentum. *Nano. Lett.* **18**, 38–42 (2018).
73. Chin, J. Y. et al. Nonreciprocal plasmonics enables giant enhancement of thin-film faraday rotation. *Nat. Commun.* **4**, 1599 (2013).
74. Fedotov, V. A. et al. Asymmetric propagation of electromagnetic waves through a planar chiral structure. *Phys. Rev. Lett.* **97**, 167401 (2006).
75. Kaelberer, T., Fedotov, V., Papasimakis, N., Tsai, D. & Zheludev, N. Toroidal dipolar response in a metamaterial. *Science* **330**, 1510–1512 (2010).
76. Papasimakis, N., Fedotov, V. A., Savinov, V., Raybould, T. A. & Zheludev, N. I. Electromagnetic

toroidal excitations in matter and free space. *Nat. Mater.* **15**, 263–271 (2016).
77. Fernandez-Corbaton, I., Nanz, S. & Rockstuhl, C. On the dynamic toroidal multipoles from localized electric current distributions. *Sci. Rep.* **7**, 7527 (2017).
78. Wegener, M. *Extreme Nonlinear Optics* (Springer-Verlag, 2005).
79. Kauranen, M. & Zayats, A. V. Nonlinear plasmonics. *Nat. Photonics* **6**, 737–748 (2012).
80. Lee, J. et al. Giant nonlinear response from plasmonic metasurfaces coupled to intersubband transitions. *Nature* **511**, 65–69 (2014).
81. Samson, Z. L. et al. Metamaterial electro-optic switch of nanoscale thickness. *Appl. Phys. Lett.* **96**, 143105 (2010).
82. Buchnev, O., Ou, J. Y., Kaczmarek, M., Zheludev, N. I. & Fedotov, V. A. Electro-optical control in a plasmonic metamaterial hybridised with a liquid-crystal cell. *Opt. Express* **21**, 1633–1638 (2013).
83. Khurgin, J. B. & Sun, G. Plasmonic enhancement of the third order nonlinear optical phenomena: figures of merit. *Opt. Express* **21**, 27460–27480 (2013).
84. Jahani, S. & Jacob, Z. All-dielectric metamaterials. *Nat. Nanotechnol.* **11**, 23–36 (2016).
85. Staude, I. & Schilling, J. Metamaterial-inspired silicon nanophotonics. *Nat. Photonics* **11**, 274–284 (2017).
86. Hermans, A. et al. On the determination of χ (2) in thin films: a comparison of one-beam second-harmonic generation measurement methodologies. *Sci. Rep.* **7**, 44581 (2017).
87. Kadic, M., Bückmann, T., Schittny, R. & Wegener, M. Metamaterials beyond electromagnetism. *Rep. Prog. Phys.* **76**, 126501 (2013).
88. Ding, Y., Liu, Z., Qiu, C. & Shi, J. Metamaterial with simultaneously negative bulk modulus and mass density. *Phys. Rev. Lett.* **99**, 093904 (2007).
89. Lee, S. H., Park, C. M., Seo, Y. M., Wang, Z. G. & Kim, C. K. Composite acoustic medium with simultaneously negative density and modulus. *Phys. Rev. Lett.* **104**, 054301 (2010).
90. Wu, Y., Lai, Y. & Zhang, Z. Q. Elastic metamaterials with simultaneously negative effective shear modulus and mass density. *Phys. Rev. Lett.* **107**, 105506 (2011).
91. Cummer, S. A., Christensen, J. & Alu, A. Controlling sound with acoustic metamaterials. *Nat. Rev. Mater.* **1**, 16001 (2016).
92. Liu, Z. et al. Locally resonant sonic materials. *Science* **289**, 1734–1736 (2000).
93. Schoenberg, M. & Sen, P. N. Properties of a periodically stratified acoustic half-space and its relation to a Biot fluid. *J. Acoust. Soc. Am.* **73**, 61–67 (1983).
94. Milton, G. W., Birane, M. & Willis, J. R. On cloaking for elasticity and physical equations with a transformation invariant form. *New J. Phys.* **8**, 248 (2006).
95. Willis, J. R. Effective constitutive relations for waves in composites and metamaterials. *Proc. Roy. Soc. Lond. A* **467**, 1865–1879 (2011).
96. Muhlestein, M. B., Sieck, C. F., Wilson, P. S. & Haberman, M. R. Experimental evidence of Willis coupling in a one-dimensional effective material element. *Nat. Commun.* **8**, 15625 (2017).
97. Bueckmann, T., Kadic, M., Schittny, R. & Wegener, M. Mechanical metamaterials with anisotropic and negative effective mass-density tensor made from one constituent material. *Phys. Status Solidi B* **252**, 1671–1674 (2015).
98. Yang, M., Chen, S., Fu, C. & Sheng, P. Optimal sound-absorbing structures. *Mater. Horiz.* **4**, 673–680 (2017).
99. Ma, G. & Sheng, P. Acoustic metamaterials: from local resonances to broad horizons. *Sci. Adv.* **2**, e1501595 (2015).
100. Liang, Z. & Li, J. Extreme acoustic metamaterial by coiling up space. *Phys. Rev. Lett.* **108**, 114301 (2012).
101. Frenzel, T. et al. Three-dimensional labyrinthine acoustic metamaterials. *Appl. Phys. Lett.* **103**, 061907 (2013).
102. Xie, Y., Konneker, A., Popa, B.-I. & Cummer, S. A. Tapered labyrinthine acoustic metamaterials for broadband impedance matching. *Appl. Phys. Lett.* **103**, 201906 (2013).
103. Krushynska, A. O., Bosia, F., Miniaci, M. & Pugno, N. M. Spider web-structured labyrinthine acoustic metamaterials for low-frequency sound control. *New J. Phys.* **19**, 105001 (2017).
104. Maurya, S. K., Pandey, A., Shukla, S. & Saxena, S. Double negativity in 3D space coiling metamaterials. *Sci. Rep.* **6**, 33683 (2016).
105. Fleury, R., Sounas, D. L., Sieck, C. F., Haberman, M. R. & Alu, A. Sound isolation and giant linear nonreciprocity in a compact acoustic circulator. *Science* **343**, 516–519 (2014).
106. Aurégan, Y. & Pagneux, V. $\mathcal{PT}$-symmetric scattering in flow duct acoustics. *Phys. Rev. Lett.* **118**, 174301 (2017).
107. Banerjee, B. *An Introduction to Metamaterials and Waves in Composites* (Taylor and Francis, 2011).
108. Walpole, L. On bounds for the overall elastic moduli of inhomogeneous systems — I. *J. Mech. Phy. Solids* **14**, 151–162 (1966).
109. Milton, G. W. Complete characterization of the macroscopic deformations of periodic unimode metamaterials of rigid bars and pivots. *J. Mech. Phy. Solids* **61**, 1543–1560 (2013).
110. Milton, G. W. & Cherkaev, A. V. Which elasticity tensors are realizable? *J. Eng. Mater. Technol.* **117**, 483–493 (1995).
111. Kadic, M., Bückmann, T., Stenger, N., Thiel, M. & Wegener, M. On the practicability of pentamode mechanical metamaterials. *Appl. Phys. Lett.* **100**, 191901 (2012).
112. Kadic, M., Schittny, R., Bückmann, T. & Wegener, M. On anisotropic versions of three-dimensional pentamode metamaterials. *New J. Phys.* **15**, 023029 (2013).
113. Bueckmann, T. et al. On three-dimensional dilational elastic metamaterials. *New J. Phys.* **16**, 033032 (2014).
114. Biot, M. Theory of propagation of elastic waves in a fluid-saturated porous solid. I. Low-frequency range. *J. Acoust. Soc. Am.* **28**, 168–178 (1956).
115. Biot, M. & Willis, D. The elastic coefficients of the theory of consolidation. *J. Appl. Mech.* **24**, 594–601 (1957).
116. Gatt, R. & Grima, J. N. Negative compressibility. *Phys. Status Solidi RRL* **2**, 236–238 (2008).
117. Qu, J., Kadic, M. & Wegener, M. Poroelastic metamaterials with negative effective static compressibility. *Appl. Phys. Lett.* **110**, 171901 (2017).
118. Qu, J., Gerber, A., Mayer, F., Kadic, M. & Wegener, M. Experiments on metamaterials with negative effective static compressibility. *Phys. Rev. X* **7**, 041060 (2017).
119. Sommerfeld, A. *Mechanics of Deformable Bodies* (Academic Press, 1950).
120. Eringen, A. *Microcontinuum Field Theories I: Foundations and Solids*. (Springer, New York, 1999). **This is a textbook on theoretical paths towards generalizing linear Cauchy elasticity**.
121. Frenzel, T., Kadic, M. & Wegener, M. Three-dimensional mechanical metamaterials with a twist. *Science* **358**, 1072–1074 (2017).
122. Rueger, Z. & Lakes, R. S. Strong cosserat elasticity in a transversely isotropic polymer lattice. *Phys. Rev. Lett.* **120**, 065501 (2018).
123. Zhu, H. et al. Observation of chiral phonons. *Science* **359**, 579–582 (2018).
124. Coulais, C., Kettenis, C. & van Hecke, M. A characteristic length scale causes anomalous size effects and boundary programmability in mechanical metamaterials. *Nat. Phys.* **14**, 40–44 (2017).
125. Kadic, M., Frenzel, T. & Wegener, M. Mechanical metamaterials: when size matters. *Nat. Phys.* **14**, 8–9 (2018).
126. Nash, L. M. et al. Topological mechanics of gyroscopic metamaterials. *Proc. Natl Acad. Sci. USA* **112**, 14495–14500 (2015).
127. Hassanpour, S. & Heppler, G. R. Theory of micropolar gyroelastic continua. *Acta Mech.* **227**, 1469–1491 (2016).
128. Carta, G., Jones, I. S., Movchan, N. V., Movchan, A. B. & Nieves, M. J. Deflecting elastic prism and unidirectional localisation for waves in chiral elastic systems. *Sci. Rep.* **7**, 26 (2017).
129. Abdoul-Anziz, H. & Seppecher, P. Strain gradient and generalized continua obtained by homogenizing frame lattices. *Math. Mech. Complex Syst.* **6**, 213–250 (2018).
130. Gudmundson, P. A unified treatment of strain gradient plasticity. *J. Mech. Phys. Solids* **52**, 1379–1406 (2004).
131. Olive, M. & Auffray, N. Symmetry classes for odd-order tensors. *J. Appl. Math. Mech.* **94**, 421–447 (2014).
132. Cordero, N. M., Forest, S. & Busso, E. P. Second strain gradient elasticity of nano-objects. *J. Mech. Phys. Solids* **97**, 92–124 (2016).
133. Liebold, C. & Mueller, W. H. Comparison of gradient elasticity models for the bending of micromaterials. *Comput. Mater. Sci.* **116**, 52–61 (2016).
134. Lecoutre, G., Daher, N., Devel, M. & Hirsinger, L. Principle of virtual power applied to deformable semiconductors with strain, polarization, and magnetization gradients. *Acta Mech.* **228**, 1681–1710 (2017).
135. Bertram, A. Compendium on gradient materials. *Redaktion* http://www.redaktion.tu-berlin.de/fileadmin/fg49/publikationen/bertram/Compendium_on_Gradient_Materials_Dec_2017.pdf (2017).
136. Wang, P., Casadei, F., Shan, S., Weaver, J. C. & Bertoldi, K. Harnessing buckling to design tunable locally resonant acoustic metamaterials. *Phys. Rev. Lett.* **113**, 014301 (2014).
137. Florijn, B., Coulais, C. & van Hecke, M. Programmable mechanical metamaterials. *Phys. Rev. Lett.* **113**, 175503 (2014).
138. Kang, S. H. et al. Complex ordered patterns in mechanical instability induced geometrically frustrated triangular cellular structures. *Phys. Rev. Lett.* **112**, 098701 (2014).
139. Bauer, J. et al. Nanolattices: an emerging class of mechanical metamaterials. *Adv. Mater.* **29**, 1701850 (2017).
140. Bertoldi, K., Vitelli, V., Christensen, J. & van Hecke, M. Flexible mechanical metamaterials. *Nat. Rev. Mater.* **2**, 17066 (2017). **This is a further reading on recent progress in 2D and 3D elastic metamaterials**.
141. Tobias, F., Claudio, F., Muamer, K., Peter, G. & Martin, W. Tailored buckling microlattices as reusable light-weight shock absorbers. *Adv. Mater.* **28**, 5865–5870 (2016).
142. Coulais, C., Teomy, E., de Reus, K., Shokef, Y. & van Hecke, M. Combinatorial design of textured mechanical metamaterials. *Nature* **535**, 529–532 (2016).
143. Schenk, M. & Guest, S. D. Geometry of miura-folded metamaterials. *Proc. Natl Acad. Sci. USA* **110**, 3276–3281 (2013).
144. Wei, Z. Y., Guo, Z. V., Dudte, L., Liang, H. Y. & Mahadevan, L. Geometric mechanics of periodic pleated origami. *Phys. Rev. Lett.* **110**, 215501 (2013).
145. Waitukaitis, S., Menaut, R., Chen, B. G.-G. & van Hecke, M. Origami multistability: from single vertices to metasheets. *Phys. Rev. Lett.* **114**, 055503 (2015).
146. Silverberg, J. L. et al. Origami structures with a critical transition to bistability arising from hidden degrees of freedom. *Nat. Mater.* **14**, 389–393 (2015).
147. Coulais, C., Sounas, D. & Alu, A. Static non-reciprocity in mechanical metamaterials. *Nature* **542**, 461–464 (2017).
148. Gao, H., Ji, B., Jaeger, I. L., Arzt, E. & Fratzl, P. Materials become insensitive to flaws at nanoscale: lessons from nature. *Proc. Natl Acad. Sci. USA* **100**, 5597–5600 (2003).
149. Schaedler, T. A. et al. Ultralight metallic microlattices. *Science* **334**, 962–965 (2011).
150. Zheng, X. et al. Ultralight, ultrastiff, mechanical metamaterials. *Science* **344**, 1373–1377 (2014).
151. Meza, L. R., Das, S. & Greer, J. R. Strong, lightweight, and recoverable three-dimensional ceramic nanolattices. *Science* **345**, 1322–1326 (2014).
152. Bauer, J., Hengsbach, S., Tesari, I., Schwaiger, R. & Kraft, O. High-strength cellular ceramic composites with 3D microarchitecture. *Proc. Natl Acad. Sci. USA* **111**, 2453–2458 (2014).
153. Bauer, J. et al. Nanolattices: an emerging class of mechanical metamaterials. *Adv. Mater.* **29**, 1701850 (2002).
154. Popovic, R. S. *Hall Effect Devices* (Institute of Physics Publishing, Philadelphia, 2004).
155. Briane, M., Milton, G. W. & Nesi, V. Change of sign of the corrector's determinant for homogenization in three-dimensional conductivity. *Arch. Ration. Mech. Anal.* **173**, 133–150 (2004).
156. Briane, M. & Milton, G. W. An antisymmetric effective Hall matrix. *SIAM J. Appl. Math.* **70**, 1810–1820 (2010).
157. Tornow, M. et al. Anisotropic magnetoresistance of a classical antidot array. *Phys. Rev. Lett.* **77**, 147–150 (1996).
158. Kadic, M., Schittny, R., Bückmann, T., Kern, C. & Wegener, M. Hall-effect sign inversion in a realizable 3D metamaterial. *Phys. Rev. X* **5**, 021030 (2015).
159. Kern, C., Kadic, M. & Wegener, M. Experimental evidence for sign reversal of the Hall coefficient in three-dimensional metamaterials. *Phys. Rev. Lett.* **118**, 016601 (2017).
160. Kern, C., Graeme, W. M., Kadic, M. & Wegener, M. Theory of the Hall effect in three-dimensional metamaterials. *New J. Phys.* **20**, 083034 (2018).
161. Bergman, D. J. & Strelniker, Y. M. Calculation of strong-field magnetoresistance in some periodic composites. *Phys. Rev. B* **49**, 16256–16268 (1994).
162. Strelniker, Y. M. & Bergman, D. J. Thermoelectric response of a periodic composite medium in the presence of a magnetic field: angular anisotropy. *Phys. Rev. B* **96**, 235308 (2017).

163. Liu, L. Feasibility of large-scale power plants based on thermoelectric effects. *New J. Phys.* **16**, 123019 (2014).
164. Schittny, R., Kadic, M., Guenneau, S. & Wegener, M. Experiments on transformation thermodynamics: molding the flow of heat. *Phys. Rev. Lett.* **110**, 195901 (2013).
165. Ros, A. et al. Brownian motion: absolute negative particle mobility. *Nature* **436**, 928–928 (2005).
166. Kern, C., Schuster, V., Kadic, M. & Wegener, M. Experiments on the parallel Hall effect in three-dimensional metamaterials. *Phys. Rev. Appl.* **7**, 044001 (2017).
167. Onsager, L. Reciprocal relations in irreversible processes. I. *Phys. Rev.* **37**, 405–426 (1931).
168. Debord, J. D. & Lyon, L. A. Thermoresponsive photonic crystals. *J. Phys. Chem. B* **104**, 6327–6331 (2000).
169. Stuart, M. A. C. et al. Emerging applications of stimuli-responsive polymer materials. *Nat. Mater.* **9**, 101–113 (2010).
170. Schroden, R. C., Al-Daous, M., Blanford, C. F. & Stein, A. Optical properties of inverse opal photonic crystals. *Chem. Mater.* **14**, 3305–3315 (2002).
171. Theato, P., Sumerlin, B. S., O'Reilly, R. K. & Epps, T. H. III Stimuli responsive materials. *Chem. Soc. Rev.* **42**, 7055–7056 (2013).
172. Skylar, T. 4D printing: multi-material shape change. *Archit. Des.* **84**, 116–121 (2014).
173. Hao, Z. et al. Light-fueled microscopic walkers. *Adv. Mater.* **27**, 3883–3887 (2015).
174. Martella, D. et al. Light activated non-reciprocal motion in liquid crystalline networks by designed microactuator architecture. *RSC Adv.* **7**, 19940–19947 (2017).
175. Momeni, F., Hassani, S. M. M., Liu, X. & Ni, J. A review of 4D printing. *Mater. Des.* **122**, 42–79 (2017).
176. Akihiro, N., Ahmed, M., Hang, Z. & Martin, M. In-gel direct laser writing for 3D-designed hydrogel composites that undergo complex self-shaping. *Adv. Sci.* **5**, 1700038 (2017).
177. Park, H. et al. Mechanical metamaterials with thermoresponsive switching between positive and negative poisson's ratios. *Phys. Status Solidi RRL* **12**, 1800040 (2018).
178. Hess, O. et al. Active nanoplasmonic metamaterials. *Nat. Mater.* **11**, 573–584 (2012).
179. Shadrivov, I., Lapine, M. & Kivshar, Y. *Nonlinear, Tunable and Active Metamaterials* (Springer, 2014).
180. Fan, K. & Padilla, W. J. Dynamic electromagnetic metamaterials. *Mater. Today* **18**, 39–50 (2015).
181. Tong, X. *Functional Metamaterials and Metadevices* (Springer, 2017).
182. Rout, S. & Sonkusale, S. *Active Metamaterials: Terahertz Modulators and Detectors* (Springer, 2017).
183. Yu, K., Fang, N.-X., Huang, G. & Wang, Q. Magnetoactive acoustic metamaterials. *Adv. Mater.* **30**, 1706348 (2018).
184. Estep, N. A., S, J., Sounas, D. L. & Alu, A. Magnetic-free non-reciprocity and isolation based on parametrically modulated coupled-resonator loops. *Nat. Phys.* **10**, 923–927 (2014).
185. Bacot, V., Labousse, M., Eddi, A., Fink, M. & Fort, E. Time reversal and holography with spacetime transformations. *Nat. Phys.* **12**, 972–977 (2016).
186. Deck-Léger, Z.-L., Akbarzadeh, A. & Caloz, C. Wave deflection and shifted refocusing in a medium modulated by a superluminal rectangular pulse. *Phys. Rev. B* **97**, 104305 (2018).
187. Halimeh, J. C., Thompson, R. T. & Wegener, M. Invisibility cloaks in relativistic motion. *Phys. Rev. A.* **93**, 013850 (2016).
188. Fang, K., Yu, Z. & Fan, S. Realizing effective magnetic field for photons by controlling the phase of dynamic modulation. *Nat. Photonics* **6**, 782–787 (2012).
189. Nassar, H., Chen, H., Norris, A. N. & Huang, G. L. Quantization of band tilting in modulated phononic crystals. *Phys. Rev. B* **97**, 014305 (2018).
190. Milton, G. W. & Mattei, O. Field patterns: a new mathematical object. *Proc. Roy. Soc. Lond. A* **473**, 20160819 (2017).
191. Xu, S. & Wu, C. Space-time crystal and space-time group. *Phys. Rev. Lett.* **120**, 096401 (2018).
192. Burckel, D. B. et al. Micrometer-scale cubic unit cell 3D metamaterial layers. *Adv. Mater.* **22**, 5053–5057 (2010).
193. Sreekanth, K. V., Luca, A. D. & Strangi, G. Experimental demonstration of surface and bulk plasmon polaritons in hypergratings. *Sci. Rep.* **3**, 3291 (2013).
194. Correa, D. et al. Negative stiffness honeycombs for recoverable shock isolation. *Rapid Prototyp. J.* **21**, 193–200 (2015).
195. Wang, Q. et al. Lightweight mechanical metamaterials with tunable negative thermal expansion. *Phys. Rev. Lett.* **117**, 175901 (2016).
196. Ozaki, M., Shimoda, Y., Kasano, M. & Yoshino, K. Electric field tuning of the stop band in a liquid-crystal-infiltrated polymer inverse opal. *Adv. Mater.* **14**, 514–518 (2002).
197. Kamenjicki, M., & Lednev, I. & Asher, S. A. Photoswitchable spirobenzopyran-based photochemically controlled photonic crystals. *Adv. Funct. Mater.* **15**, 1401–1406 (2005).
198. Cui, T. J., Qi, M. Q., Wan, X., Zhao, J. & Cheng, Q. Coding metamaterials, digital metamaterials and programmable metamaterials. *Light Sci. Appl.* **3**, e218 (2014).
199. Zhao, J. et al. Controlling spectral energies of all harmonics in programmable way using time-domain digital coding metasurface. Preprint at *arXiv* https://arxiv.org/abs/1806.04414 (2018).
200. Gracias, D. H. Stimuli responsive self-folding using thin polymer films. *Curr. Opin. Chem. Eng.* **2**, 112–119 (2013).
201. Laude, V. et al. Extraordinary nonlinear transmission modulation in a doubly resonant acousto-optical structure. *Optica* **4**, 1245–1250 (2017).
202. Roy, D., Cambre, J. N. & Sumerlin, B. S. Future perspectives and recent advances in stimuli-responsive materials. *Prog. Polym. Sci.* **35**, 278–301 (2010).
203. Courjal, N. et al. Acousto-optically tunable lithium niobate photonic crystal. *Appl. Phys. Lett.* **96**, 131103 (2010).
204. Shin, D. et al. Scalable variable-index elasto-optic metamaterials for macroscopic optical components and devices. *Nat. Commun.* **8**, 16090 (2017).
205. Babaee, S., Viard, N., Wang, P., Fang, N. X. & Bertoldi, K. Harnessing deformation to switch on and off the propagation of sound. *Adv. Mater.* **28**, 1631–1635 (2016).
206. Zhang, X., Liu, J., Chu, M. & Chu, B. Flexoelectric piezoelectric metamaterials based on the bending of ferroelectric ceramic wafers. *Appl. Phys. Lett.* **109**, 072903 (2016).
207. Weissman, J. M., Sunkara, H. B., Tse, A. S. & Asher, S. A. Thermally switchable periodicities and diffraction from mesoscopically ordered materials. *Science* **274**, 959–963 (1996).
208. Kubo, S. et al. Tunable photonic band gap crystals based on a liquid crystal-infiltrated inverse opal structure. *J. Am. Chem. Soc.* **126**, 8314–8319 (2004).
209. Nicolaou, Z. G. & Motter, A. E. Mechanical metamaterials with negative compressibility transitions. *Nat. Mater.* **11**, 608–13 (2012).
210. Qu, J., Kadic, M., Naber, A. & Wegener, M. Micro-structured two-component 3D metamaterials with negative thermal-expansion coefficient from positive constituents. *Sci. Rep.* **7**, 40643 (2017).
211. Zhang, H., Guo, X., Wu, J., Fang, D. & Zhang, Y. Soft mechanical metamaterials with unusual swelling behavior and tunable stress-strain curves. *Sci. Adv.* **4**, eaar8535 (2018).
212. Kamenjicki, M., Ladnev, I. K., Mikhonin, A., Kesavamoorthy, R. & Asher, S.-A. Photochemically controlled photonic crystals. *Adv. Funct. Mater.* **13**, 774–780 (2003).

Acknowledgements
The authors acknowledge stimulating discussions with C. Rockstuhl and C. Kern (Karlsruhe Institute of Technology (KIT)). M.K. acknowledges support by the Engineering and Innovation through Physical Sciences, High-technologies and Cross-disciplinary Research (EIPHI) Graduate School (contract ANR-17-EURE-0002) and the French Investissements d'Avenir program, the I-SITE Bourgogne Franche-Comté (BFC) project (contract ANR-15-IDEX-03). G.W.M. thanks the National Science Foundation for support via grant DMS-1211359 and DMS-1814854. M.W. acknowledges support by the Excellence Cluster '3D Matter Made to Order', the Helmholtz program 'Science and Technology of Nanosystems' (STN), the Karlsruhe School of Optics & Photonics (KSOP) and the 'Virtual Materials Design' (VIRTMAT) project of KIT.

Author contributions
All authors contributed to all aspects of manuscript preparation, revision and editing.

Competing interests
The authors declare no competing interests.

Publisher's note
Springer Nature remains neutral with regard to jurisdictional claims in published maps and institutional affiliations.